Rock-magnetic parameters and heavy metal distribution of the El Fraile I tailings (Guerrero, Mexico)

Parámetros de magnetismo de roca y distribución de metales pesados de los relaves mineros de la presa El Fraile I (Guerrero, México)

María del Sol **Hernández-Bernal**[1], Nayeli **Pérez Rodríguez**[2], Juan **Morales**[2,*], Avto **Goguitchaichvili**[2]

[1] Escuela Nacional de Estudios Superiores, Unidad Morelia, Universidad Nacional Autónoma de México, 58190, Morelia, Michoacán, México.

[2] Laboratorio Universitario de Geofísica Ambiental, Instituto de Geofísica Unidad Michoacán, Universidad Nacional Autónoma de México, Antigua Carretera a Pátzcuaro No. 8701, Col. Ex Hacienda de San José de la Huerta, C.P. 58190 Morelia, Michoacán, México.

* Corresponding author: (J. Morales)
jmorales@igeofisica.unam.mx

How to cite this article:
Hernández-Bernal, M. S., Pérez Rodríguez,N., Morales, J., Goguitchaichvili, A., 2024, Rock-magnetic parameters and heavy metals distribution of the El Fraile I tailings (Guerrero, Mexico): Boletín de la Sociedad Geológica Mexicana, 76 (3), A230124. http://dx.doi.org/10.18268/BSGM2024v76n3a230124

Manuscript received: January 11, 2023
Corrected manuscript received: February 7, 2024
Manuscript accepted: February 21, 2024

Peer Reviewing under the responsibility of Universidad Nacional Autónoma de México.

ABSTRACT

As a result of the mining activity at Taxco, seven mining waste dams have been generated, which could represent severe health problems for the community and environment. The study's goal comprises the El Fraile I mining-wastes dam (the oldest of the region), located south of Taxco de Alarcón, in the northern sector of the Guerrero State, Mexico. In this investigation, we present the results of a vertical magnetic-parameters prospecting and chemical characterization of 26 tailing samples from the El Fraile I. Magnetic-method results stand out diverse deposit layers of variable mineral concentration and composition, as easily identified in the stratigraphic column. The old dam's long evolution period is corroborated by the variable and much lower than 1 S_{-300} ratio values (high oxidation degree of the magnetic mineralogy) and the mostly acid pH character through the whole dam. Most maximum potential toxic elements concentration values are under the maximum permissible levels for agriculture/residential use, except for those of Pb, Cu, and Zn. An advantageous proxy method for a quick and cost-effective heavy metal evaluation of mining-wastes dams results from simple sample preparation and fast magnetic and elemental concentration estimations, together with a suitable systematic sampling distribution.

Keywords: rock-magnetic parameters, potentially toxic elements, Taxco tailings, Guerrero state.

RESUMEN

Como resultado de la actividad minera en Taxco se han generado siete represas de desechos mineros, lo que podría representar graves problemas de salud para la comunidad y el medio ambiente. El objetivo del estudio comprende la presa de desechos mineros El Fraile I (la más antigua de la región), ubicada al sur de Taxco de Alarcón, en el sector norte del estado de Guerrero, México. En esta investigación presentamos los resultados magnéticos y la caracterización elemental de una prospección vertical de 26 muestras de relaves de El Fraile I. A partir de los resultados del método magnético se destacan diversas capas de depósito de concentración y composición magnética variable, claramente identificables en la columna estratigráfica. El largo período de evolución de la antigua presa podría estar asociado con el alto grado de oxidación de la mineralogía magnética, con valores del parámetro S_{-300} mucho menores a 1, y el pH predominantemente ácido en toda la presa. La mayoría de los valores máximos de concentración de elementos potencialmente tóxicos están por debajo de los niveles máximos permitidos para uso agrícola/residencial, excepto los de Pb, Cu y Zn. Un método alternativo y ventajoso para una evaluación rápida y rentable de las presas de desechos mineros resulta de una preparación simple de muestras y estimaciones rápidas de concentración magnética y elemental, junto con una distribución sistemática adecuada del muestreo.

Palabras clave: parámetros de magnetismo de roca, elementos potencialmente tóxicos, relaves de Taxco, estado de Guerrero.

http://dx.doi.org/10.18268/BSGM2024v76n3a230124

1. Introduction

Among the different economic activities in Mexico, mining stands as one of the most traditional of them, practiced since pre-Hispanic times (Pollard, 1987; Maldonado and Rehren, 2009). It is also a regional expansion source since the Colony and plays a critical modernization and expansion role, contributing 2.05% of the country's gross domestic product (Secretaría de Economía, 2024), by supplying raw materials to virtually all sorts of industries (*e.g.*, construction, metallurgical, steel, chemistry, electronics).

Due to its long mining history of more than 450 years (Corona-Chávez *et al.*, 2010), Taxco de Alarcón rises as one of the most important Mexican mining towns. It is located in the Guerrero State's northern area (Figure 1). The Taxco Mining District (TMD) is situated south of Taxco de Alarcón. Throughout the colonial period (1521-1810), Taxco mines produced huge silver and gold amounts to be considered among America's richest mines (Talavera-Mendoza *et al.*, 2005). During this period, 5.6 Mt of tailings were generated and deposited in two valleys near the Cacalotenango River (Dótor-Almazán *et al.*, 2017).

Its extensive mining history has produced seven mining waste deposits in the region (El Fraile I, La Concha, El Solar, Guerrero I, Guerrero II, Los Jales, and San Antonio), encompassing more than 55 million tons (Dótor-Almazán *et al.*, 2017).

The El Fraile I impoundment is an abandoned tailings dam (470 m × 372 m × 60 m) located 5 km SW of Taxco, showing a high oxidation degree and a yellow-reddish color. It was formed from the exploitation of Ag-Cu-Pb-Zn ores during 1940-1970 (Talavera-Mendoza *et al.*, 2016).

However, this activity also has some negative impacts on the environment and health (Armienta *et al.*, 2003; Ramos-Arroyo *et al.*, 2004; Talavera-Mendoza *et al.*, 2005), which frequently represent a severe problem for mining districts. Such waste accumulations have great polluting potential due to their high potentially toxic element (PTE) concentrations, as reported in various studies like Armienta *et al.* (2003), Talavera-Mendoza *et al.*

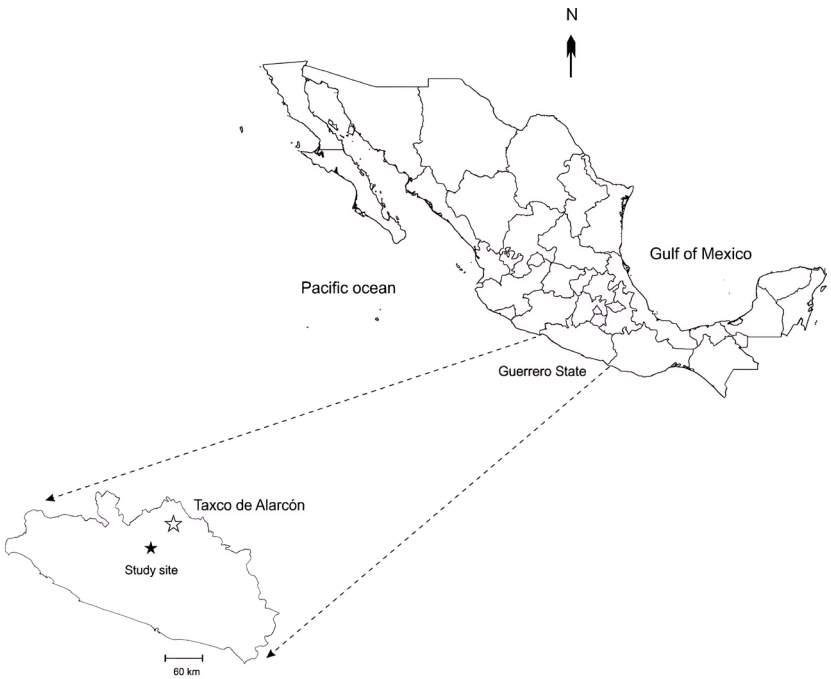

Figure 1 Location map of the study area. The hollow star highlights the Taxco de Alarcón locality, while the solid one indicates the El Fraile I tailings.

http://dx.doi.org/10.18268/BSGM2024v76n3a230124

(2005), Talavera-Mendoza *et al.* (2006), Méndez y Armienta (2012). For this reason, the study of the distribution and concentration of potentially toxic elements contained in mining wastes (tailings) is currently an issue of significant relevance (Talavera-Mendoza *et al.*, 2006).

Although different investigations: Armienta *et al.* (2003), Talavera-Mendoza *et al.* (2005), Dótor-Almazán *et al.* (2017), have been carried out on mine tailings in Taxco, waste-dump physical characteristics (color, oxidation state, etc.) on the one hand, and a limited number of samples per waste-dump (10, between 5 - 15, and 2, respectively) on the other hand, seems to have guided the sampling strategy, rather than a systematic and an exhaustive one. The low number of samples per waste dump taken could be justified due to standard methodologies used normally require ultra-pure facilities, high-purity reagents, and long processing time, making them generally expensive. Therefore, an alternative economic and rapid procedure allowing reliable PTE concentration estimation would be desirable; this would allow economic resources, time, and effort to be directed toward areas with the most significant impact or interest.

Different investigations have shown the correlation between magnetic susceptibility and heavy metal content (Petrovsky *et al.*, 1998; Petrovsky *et al.*, 2001; Ďurža, 1999; Shu *et al.*, 2001). This correlation has been attributed to the incorporation of heavy metal elements into the lattice structure of the ferrimagnetics during combustion, or alternatively to their adsorption onto the surface of the ferrimagnetics present in the environments (Petrovsky *et al.*, 1998).

Even though magnetic methods are now broadly applied in most areas of environmental investigation as a proxy for heavy metal pollution in industrial (*e.g.*, Petrovsky *et al.*, 1998; Petrovsky *et al.*, 2001; Ďurža, 1999) and urban regions (*e.g.*, Shu *et al.*, 2001; Aguilera *et al.*, 2020), mining wastes, nevertheless, have hardly been investigated by magnetic methods (Matasova *et al.*, 2005).

In the case of Mexican mining wastes, magnetic methods have only been systematically

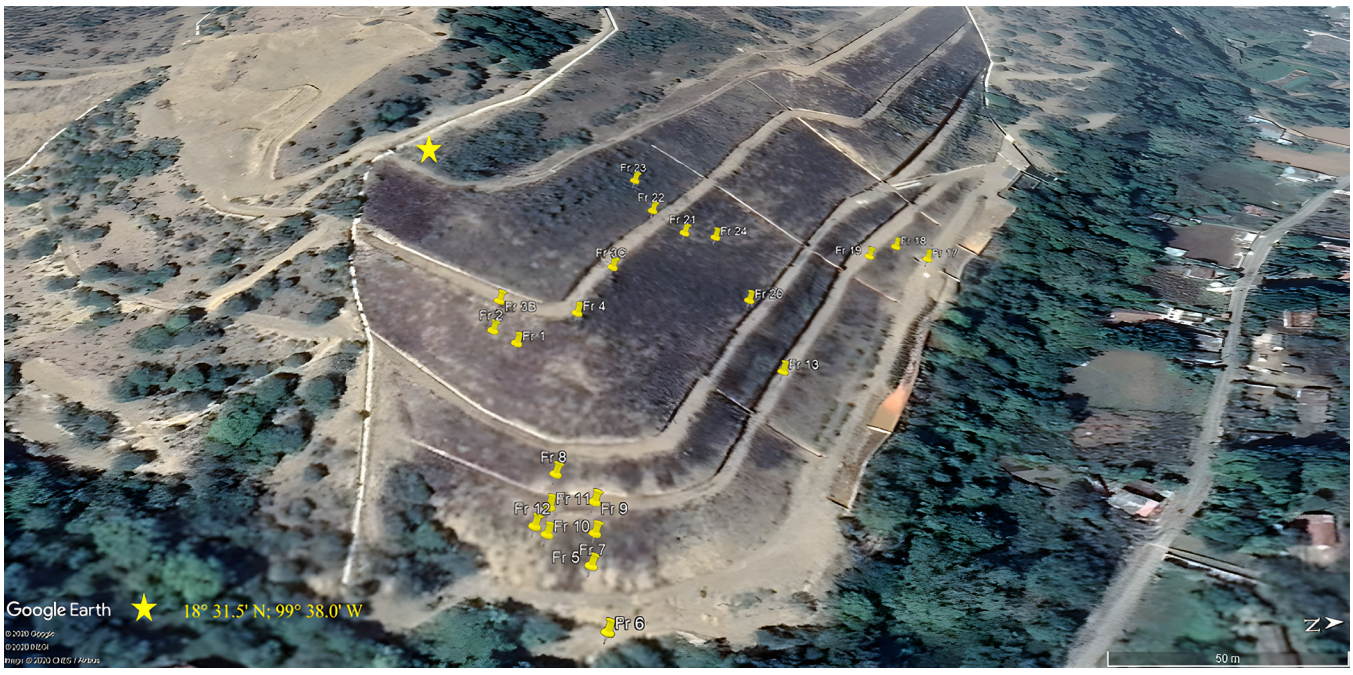

Figure 2 **Distribution of the sampling points at the El Fraile I dam.**

http://dx.doi.org/10.18268/BSGM2024v76n3a230124

employed in a metallurgical area in the San Luis Potosí State, Mexico (Pérez *et al.*, 2014), and in two western Mexico mining districts: Tlalpujahua-El Oro (Morales *et al.*, 2016), and Angangueo (Hernández-Bernal *et al.*, 2016).

In this study, the results of a methodical and comprehensive rock-magnetic and geochemical vertical survey of the El Fraile I mining-waste deposits (the oldest of the region) are presented, emphasizing their variations with the dam's depth. To achieve this aim, magnetic, physicochemical, and geochemical methods were applied.

2. Materials and methods

2.1. MATERIALS

Twenty-six tailing samples from the El Fraile I dam were collected during a field campaign at the TMD. A vertical (from top to dam's base) sampling was carried out, visually identifying the different horizons. At each horizon, approximately half a kilogram was collected and deposited into previously labeled and georeferenced polyethylene bags. Figure 2 shows the sampling points at the El Fraile I dam. The samples were kept for two weeks in a dry room away from direct sunlight and wind to avoid possible microorganism growth and cross-contamination at the laboratory facilities.

Mineralogy identification was carried out by microscopic observation of the samples spread on a petri dish. Sample preparation consisted of manually crushing ~250 g of the sample up to a particle size of clay using an agate mortar.

2.2. MAGNETIC METHODS

Half of the material of each bag was manually crushed using an agate mortar and sieved using a #10 plastic mesh (nominal aperture of 2 mm). Standard paleomagnetic acrylic cubes (8 cm^3) were filled with the milled samples for magnetic analysis.

An assortment of standard magnetic techniques was employed to magnetically characterize the samples under study:

(i) Magnetic susceptibility measurements at low (κ_{LF}) and high (κ_{HF}) frequency using a Bartington MS2 susceptibilimeter. From these low- and high-frequency results, the percent frequency-dependent magnetic susceptibility was determined (Dearing *et al.*, 1996).

$$\kappa_{FD}\% = \frac{100\ x\ (\kappa_{LF} - \kappa_{HF})}{\kappa_{LF}} \quad (1)$$

(ii) Induction of a laboratory anhysteretic magnetization (ARM) through the superposition of a 100 mT AC magnetic field over a 50 µT DC magnetic field using an AGICO LDA 3 demagnetizer. (iii) Stepwise acquisition of isothermal remanent magnetization (IRM) curves up to 1 T using an ASC Scientific IM-10 pulse magnetizer. Magnetization acquired at this last step was considered as saturation isothermal magnetization (SIRM). (vi) Backfield magnetization induction at 300 mT ($IRM_{-0.3\ T}$) for the S_{-300} ratio estimation employing the following formula (Thompson and Oldfield, 1986):

$$S_{-300} = -\frac{IRM_{-300T}}{SIRM} \quad (2)$$

(v) Acquisition of magnetization vs temperature (M−T) curves using a variable field translation balance (VFTB) up to 600°C, at a heating/cooling rate of 20°C/min.

In all cases, the remanent magnetizations were measured using an Agico JR-6 spinner magnetometer.

2.3. ELEMENTAL COMPOSITION

Pressed-pellet samples were prepared for geochemical analysis by mixing and homogenizing within the same agate mortar 3 g of the milled material with 0.5 g of wax-C micro powder (Hoechst). A 3-mm-diameter stainless-steel die and an Atlas

http://dx.doi.org/10.18268/BSGM2024v76n3a230124

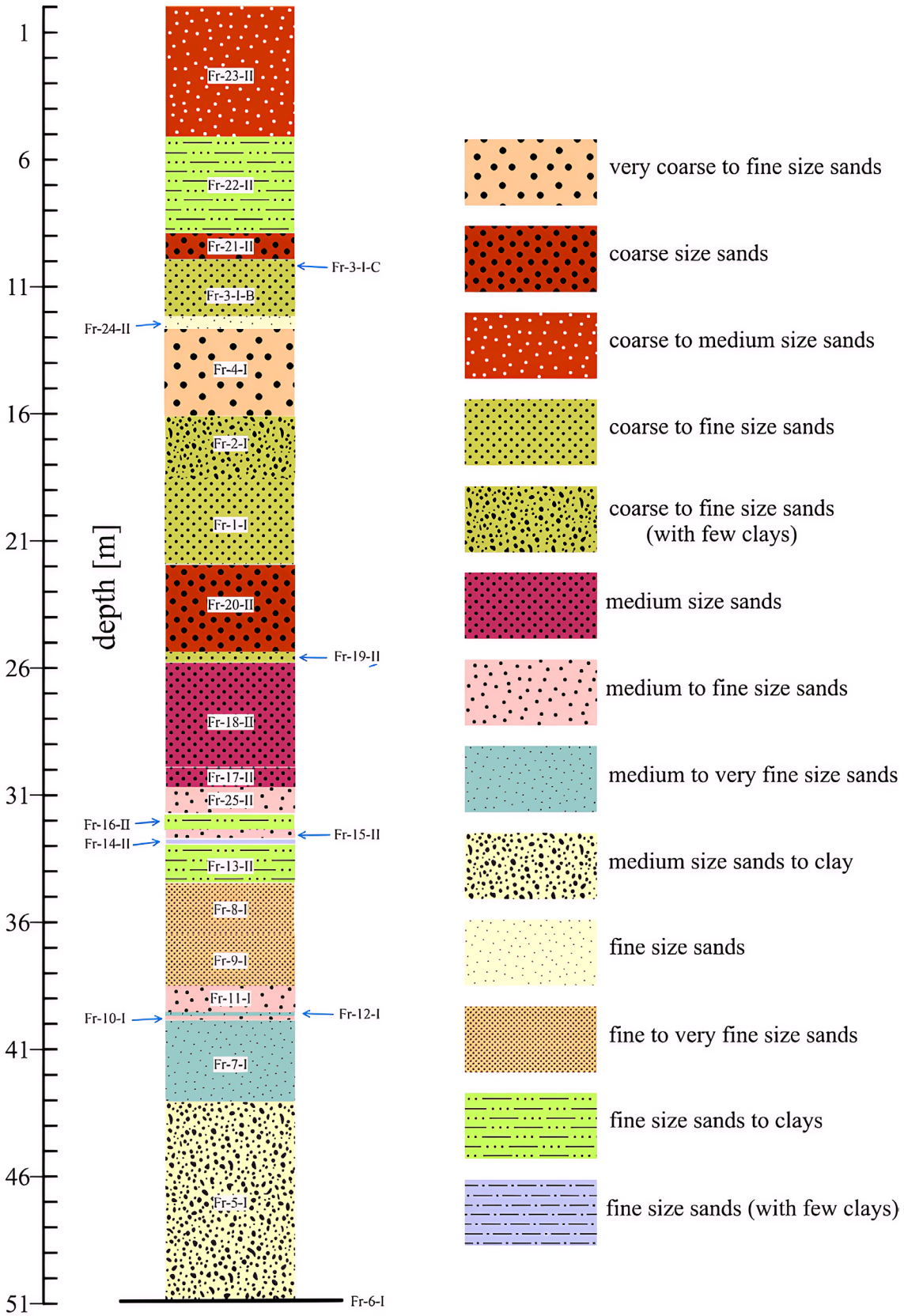

Figure 3 El Fraile I stratigraphic column.

http://dx.doi.org/10.18268/BSGM2024v76n3a230124

(Specac) hydraulic press were employed for pressing up to 20 tons for two minutes the material deposited into the die.

The samples' chemical composition (both major and trace elements) was obtained through energy dispersive (ED) X-ray fluorescence using a Xenemetrix 50-kV-tube X-Calibur ED-XRF spectrometer.

2.4. PHYSICOCHEMICAL ANALYSIS

Five grams of the milled material were dissolved into 50 ml of distilled water and stirred for half an hour for physicochemical analyses. An HI 2020 multi-parametric kit was used for the physical-chemical properties: pH and electrical conductivity (EC) determination.

All analyses were carried out at the Laboratorio Universitario de Geofísica Ambiental (LUGA) facilities, Instituto de Geofísica Unidad Michoacán.

3. Results

3.1. PHYSICAL AND MAGNETIC RESULTS

The El Fraile I dam's surface shows a series of contrasting and intercalated red, ochre-reddish, green, ochre-greenish, and green-yellowish layers (Figure 3). This sequence presents an alternation of partially well-consolidated sand layers of coarse,

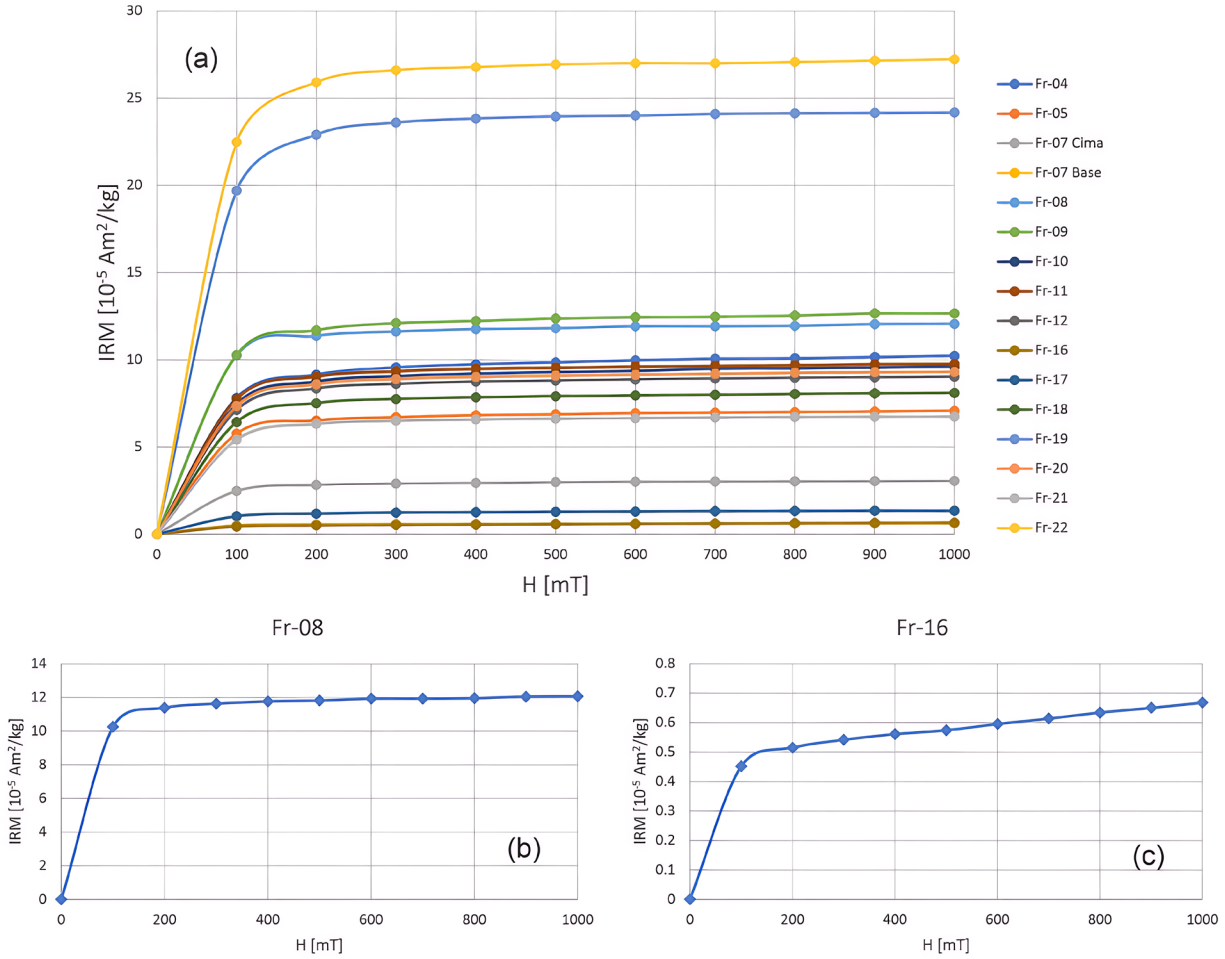

Figure 4 Representative IRM plots for the El Fraile I dam (a). Example of a saturated (b) and unsaturated (c) IRM plot.

http://dx.doi.org/10.18268/BSGM2024v76n3a230124

Table 1. Textural and mineralogical characteristics. Py: pyrite; Qz: quartz; Hm: hematite; Mt: magnetite; Ca: calcium; Gy: gypsum.

Depth [m]	Sample	Color	Size	Consolidation state	Mineralogy	Structure
0.0	Fr 23-II	Reddish	coarse to medium size sands	consolidated	Qz + Hm + Mt	
5.2	Fr 22-II	Yellow greenish	fine size sands to clays	slight consolidated	Qz + Hm + Mt	
8.9	Fr 21-II	Ochre-reddish	coarse size sands	well consolidated	Qz + Hm + Mt + Gy	
10.0	Fr 3-IC	Green yellowish	coarse to fine size sands	partially consolidated	Qz + Hm + Mt	
10.3	Fr 3-IB	Green yellowish	coarse to fine size sands			
12.2	Fr 24-II	Greenish	fine sands	partially consolidated	Qz + Hm + Mt	
12.7	Fr 4-I	Green yellowish	very coarse to fine size sands	partially consolidated	Qz + Mt	
16.1	Fr 2-I	Green yellowish	coarse to fine size sands (few clays)	partially consolidated	Qz + Mt	peak shape structures
18.5	Fr 1-I	Red ochre	coarse to fine size sands	partially consolidated	Qz + Hm + Mt + Ca	
21.9	Fr 20-II	Red ochre	coarse size sands	consolidated	Qz + Hm + Mt + Ca + Gy	peak shape structures
25.4	Fr 19-II	Red greenish	coarse to fine size sands	well consolidated	Qz + Hm + Mt + Ca + Gy	
25.7	Fr 18-II	Reddish	medium size sands	well consolidated	Qz + Hm + Ca + Gy	fine lamellae
30.0	Fr 17-II	Reddish	medium size sands	well consolidated	Qz + Hm + Mt + Ca	fine lamellae
30.6	Fr 25-II	Ochre-reddish	medium to fine size sands	consolidated	Qz + Hm + Mt + Ca + Gy	
31.8	Fr 16-II	Greenish	fine size sands to clays	partially consolidated	Qz + Hm + Mt	peak shape structures
32.3	Fr 15-II	Ochre-reddish	medium size sands to clays	consolidated	Qz + Hm + Gy	
32.7	Fr 14-II	Red	medium size sands - clays	well consolidated	Qz + Hm + Ca + Gy	peak shape structures
33.0	Fr 13-II	Green ochre	fine sands to clays	consolidated	Qz + Hm + Ca	peak shape structures
34.5	Fr 8-I	Red	fine to very fine size sands	well consolidated	Qz + Hm + Mt + Ca	
36.5	Fr 9-I	Ochre	fine to very fine size sands	consolidated	Qz + Hm + Ca + Gy	
38.5	Fr 11-I	Light brown reddish	medium size sands - clays	consolidated	Qz + Hm + Mt + Ca + Gy	peak shape structures
39.6	Fr 12-I	Ochre-reddish	medium to very fine size sands	petrified	Qz + Mt + Py + Ca + Gy	
39.7	Fr 10-I	Ochre-reddish	medium to fine size sands	petrified	Qz + Hm + Ca + Gy	
39.9	Fr 7-I	Green yellowish	medium to very fine size sands	well consolidated	Qz + Hm + Ca + Gy	peak shape structures
43.1	Fr 5-I	Yellow reddish	medium size sands - clays	partially consolidated	Qz + Hm + Ca + Gy	peak shape structures
50.9	Fr 6_I	Red	medium to fine size sands	well consolidated	Qz + Hm + Ca + Gy	peak shape structures

http://dx.doi.org/10.18268/BSGM2024v76n3a230124

medium, and fine grain sizes. Table 1 summarizes the textural and mineralogical characteristics of the analyzed samples.

IRM acquisition curves show that (in most cases) low fields between 200-300 mT can produce IRM values close to 90 % of saturation (Figure 4a, 4b), pointing to low coercivity minerals as remanence carriers. In some other cases, IRM acquisition curves display a slight increase at higher fields, possibly related to a small contribution of a high coercivity mineral, likely hematite (Figure 4c).

From the M-T curves, it is evident that magnetite or low Ti titanomagnetite (Tc ~ 575°C) is the main responsible for the magnetization. In the specific case of sample Fr-2-I (Figure 5b), a notorious Hopkinson peak is observed, which indicates the magnetic carrier is pure magnetite. Also observed are intermediate temperature (Tc < 500°C) magnetic phases, which are not present at the cooling branch (Figure 5a, 5c). Quite irreversible M-T curves are obtained in almost all samples analyzed, which suggests the formation of new magnetic mineralogy.

Magnetic susceptibility shows an average value of 1 x 10^{-3} through the entire vertical profile (~ 50-m-depth), with a moderate peak value at 8.9 m, and other three more pronounced peaks at intermediate depths of 25.4 m, 30.6 m, and 32.3 m (Figure 6a). The aforementioned peak values are associated with reddish-ochre color layers.

ARM acquisition curves show a similar trend to that followed by κ, except in the intervals from 10 to 22 and 35 to 40 m depth (Figure 6b). ARM/κ_{LF} curves show a marked peak at 16.1 m depth, which is not present at the ARM plot (Figure 6c). A general fining of the magnetic grain-size will

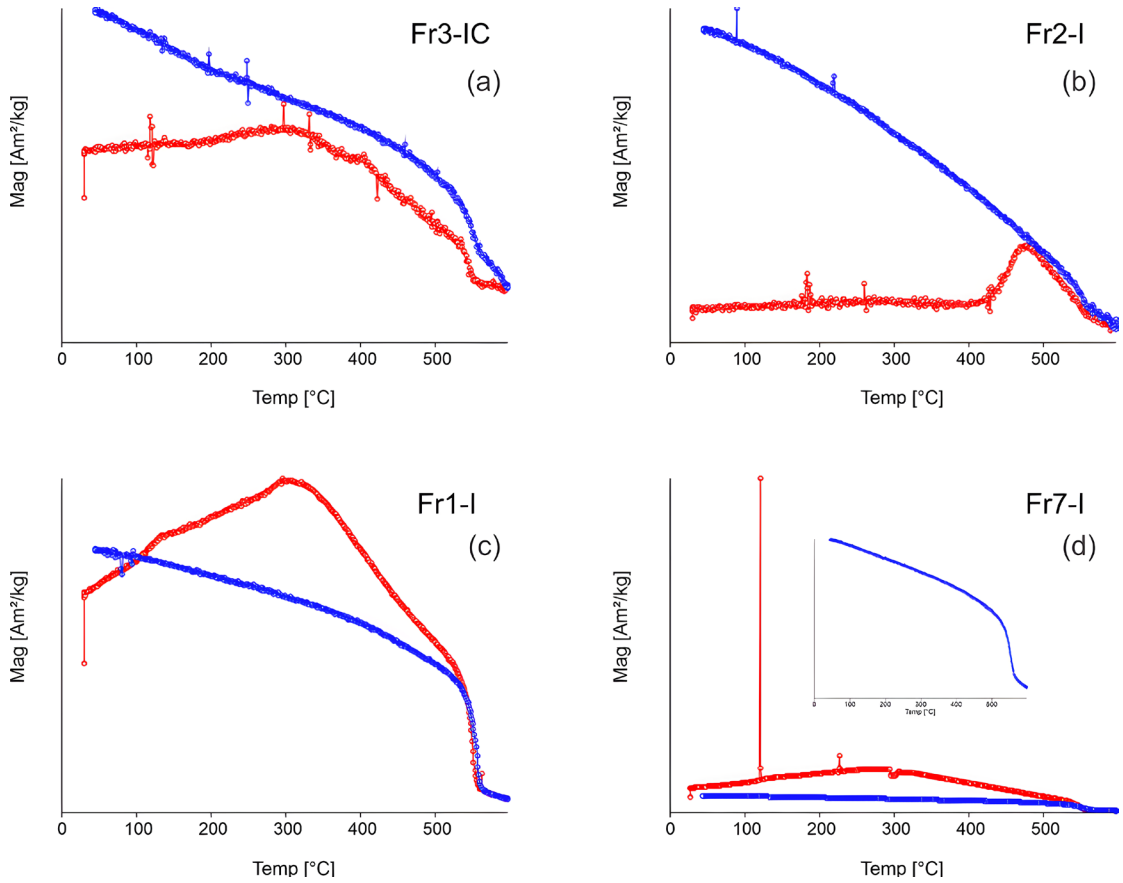

Figure 5 Representative M–T curves of the samples from the El Fraile I dam, collected at (a) 10.0, (b) 16.0, (c) 18.5, and (d) 39.9 m depths. The inset in (d) shows that the plot is similar to that displayed in (c). Red/blue branch corresponds to the heating/cooling process.

http://dx.doi.org/10.18268/BSGM2024v76n3a230124

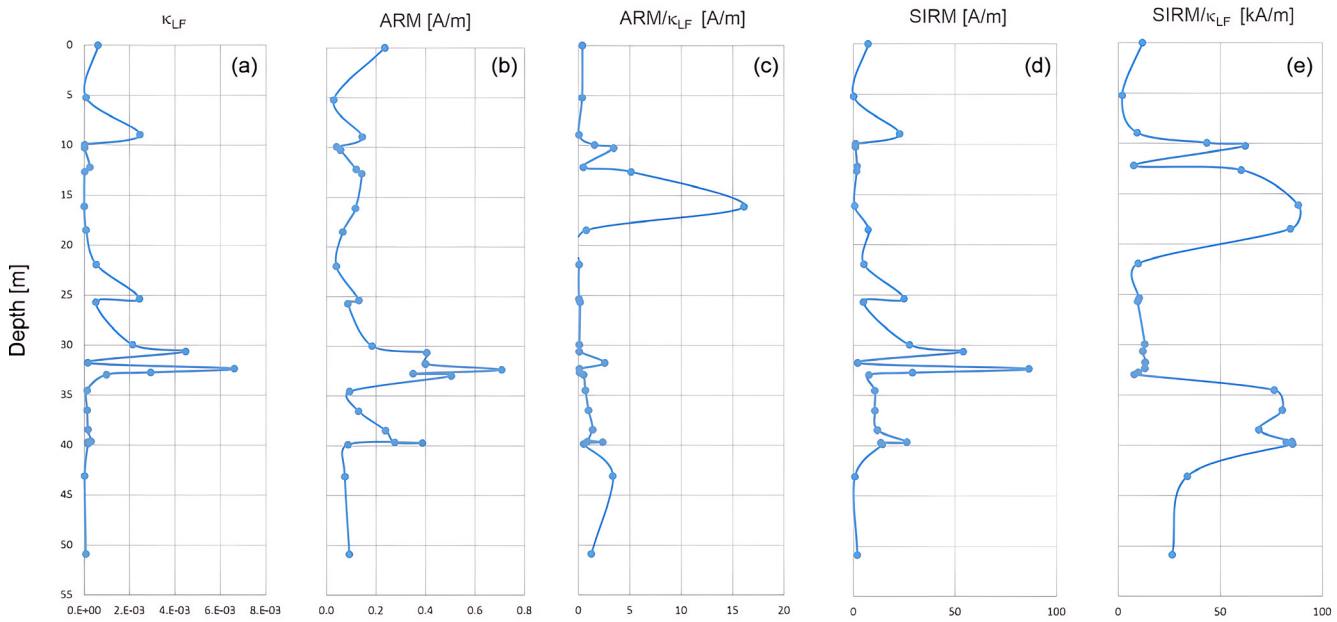

Figure 6 Concentration, grain-size, and composition dependent rock-magnetic parameters in the vertical ground profile of the El Fraile I dam.

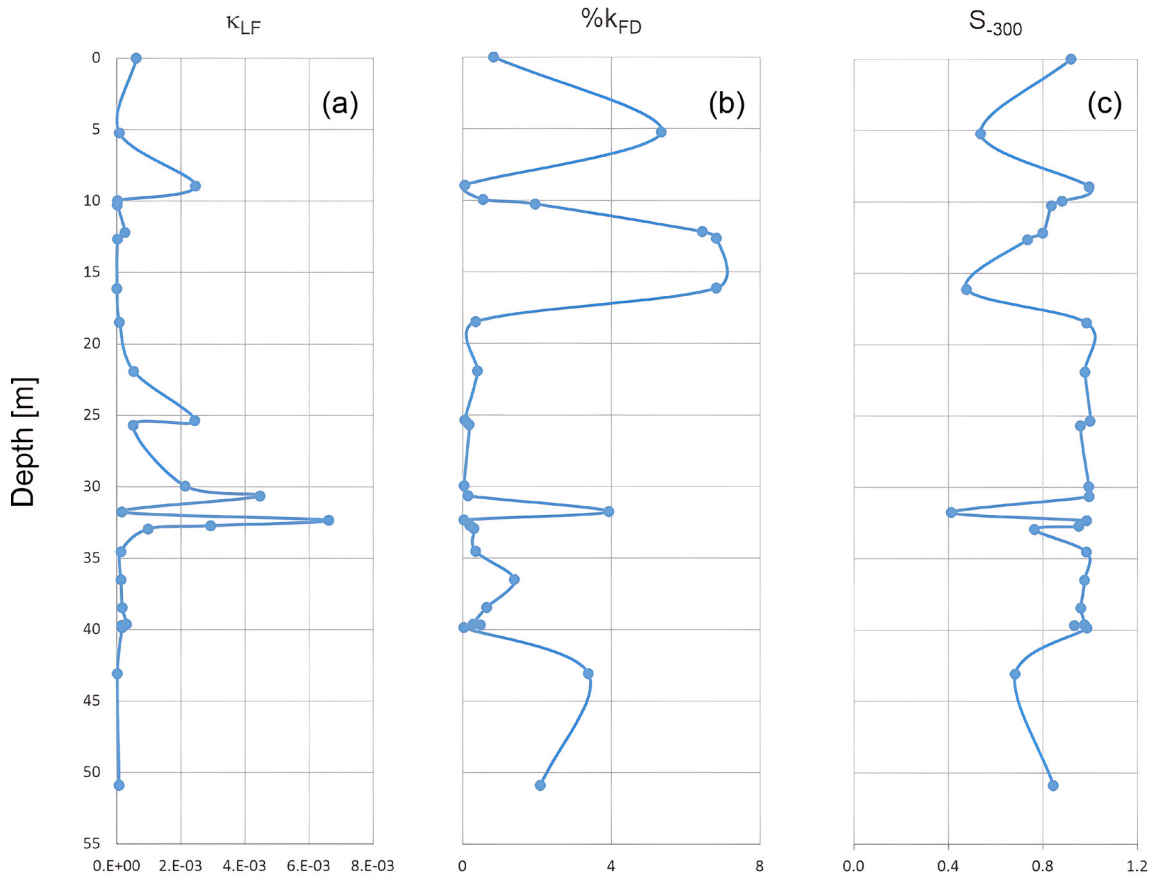

Figure 7 (a) Volume magnetic susceptibility κ_{LF}, (b) κ_{FD}%, and (c) S_{-300} ratio in the vertical ground profile of the El Fraile I dam.

http://dx.doi.org/10.18268/BSGM2024v76n3a230124

show an increase in this ratio (Vigliotti *et al.*, 2008).

A very similar tendency to that of κ is followed by the SIRM plot (Figure 6d). The above-mentioned (moderate and more pronounced) peak values observed in the κ plot are also present in the SIRM log, but not in the SIRM/κ_{LF} plot, indicating a concentration- rather than a composition-variation origin of these out-of-trend values. On the contrary, two noticeable peaks at the intervals 10.0 to 18.5 and 34.5 to 39.9 m depth are seen in the SIRM/κ_{LF} plot (Figure 6e), which suggests a composition- rather than a concentration-variation origin of these out-of-trend values. These peak values could also be interpreted as variations in the grain size of the magnetite (Thompson *et al.*, 1980; Evans and Heller, 2003).

κ_{FD}% shows more considerable variations, up to 7% (Figure 7b), especially at the upper part of the dam. These high κ_{FD}% values suggest a significant contribution of (fine particle-size) superparamagnetic ferrimagnetic minerals −in good agreement with the stratigraphic column−, especially at the dam's upper part (12.2-18.5 m-depth), and with the peak value (16.1 m depth) present in the ARM/κ_{LF} plot. The middle part is characterized by close to zero values.

Large variations (0.92-0.48) of the S_{-300} ratio are observed at the upper part of the El Fraile I dam (Figure 7c), particularly at the interval 12.2-18.5 m-depth, suggesting variable and significant hematite contribution. The middle part shows a more consistent behavior with an average value of 0.92%, except at 31.8 m depth. Worth noting is that maxima in the κ_{FD}% plot are associated with minima at the corresponding S_{-300} plot.

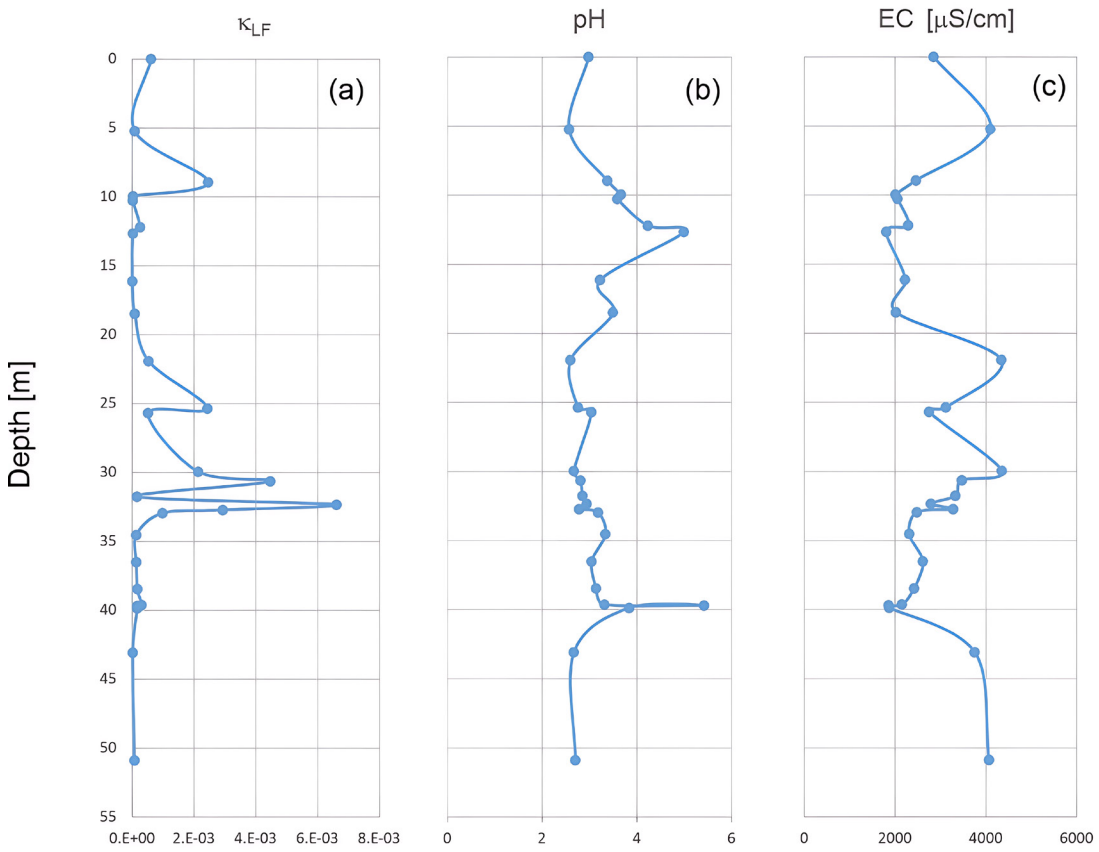

Figure 8 Corresponding physicochemical parameters (pH and EC) in the vertical ground profile of the El Fraile I dam. Figure 5a is again reproduced for comparison purposes

http://dx.doi.org/10.18268/BSGM2024v76n3a230124

Table 2. Elemental composition and statistical description of κ_{LF} and PTEs concentration in the El Fraile tailing samples. Concentration values in mg/kg, except for Fe (wt./%). RBC: Regional background concentration; MPL: Maximum permissible levels according to SEMARNAT (2007); AEF: Average enrichment factor; N.A.: Not available.

Depth [m]	Sample	κ_{lf} [unitless]	Pb	V	Ni	Cu	Zn	Fe
0.0	Fr 23-II	6.13E-04	7892.6	33.8	18.4	185.1	585.9	18.5
5.2	Fr 22-II	8.12E-05	3824.1	40.8	23.5	52.9	999.0	9.9
8.9	Fr 21-II	2.46E-03	8041.1	29.7	16.4	217.3	1786.0	13.4
10.0	Fr 3-I C	2.61E-05	5514.3	46.0	26.3	72.8	377.4	14.3
10.3	Fr 3-I B	1.67E-05	3876.8	40.6	22.6	62.8	163.6	10.6
12.2	Fr 24-II	2.54E-04	6414.0	28.3	0.5	138.0	283.8	12.5
12.7	Fr 4-I	2.79E-05	6509.5	30.3	22.6	98.3	520.0	13.1
16.1	Fr 2-I	7.30E-06	8423.2	40.0	29.0	132.3	586.0	10.7
18.5	Fr 1-I	8.77E-05	5828.5	35.8	24.2	163.1	744.5	17.4
21.9	Fr 20-II	5.33E-04	5094.6	38.0	14.9	151.2	1888.1	20.0
25.4	Fr 19-II	2.44E-03	6214.8	32.0	0.0	155.0	427.5	15.0
25.7	Fr 18-II	5.15E-04	5788.1	26.3	0.0	131.8	1231.5	15.4
30.0	Fr 17-II	2.13E-03	5655.8	21.1	5.9	169.4	2744.7	14.1
30.6	Fr 25-II	4.47E-03	5233.5	23.0	6.9	158.8	985.3	10.4
31.8	Fr 16-II	1.56E-04	4294.8	14.7	18.3	148.1	866.6	9.7
32.3	Fr 15-II	6.61E-03	8022.0	23.1	15.4	277.2	2008.3	14.1
32.7	Fr 14-II	2.94E-03	5990.1	17.3	11.0	145.3	626.5	15.0
33.0	Fr 13-II	9.85E-04	8642.8	26.2	2.5	169.5	370.7	11.6
34.5	Fr 8-I	1.38E-04	5660.9	34.9	17.2	103.7	1074.6	15.9
36.5	Fr 9-I	1.32E-04	5772.7	24.1	17.7	80.8	1103.2	18.5
38.5	Fr 11-I	1.72E-04	6693.3	47.9	22.1	261.2	967.1	18.9
39.6	Fr 12-I	3.09E-04	5906.7	33.2	0.0	99.8	544.8	18.8
39.7	Fr 10-I	1.64E-04	4479.6	25.3	15.8	113.4	1214.2	21.0
39.9	Fr 7-I	1.67E-04	4607.7	30.7	19.6	88.5	261.5	14.1
43.1	Fr 5-I	2.23E-05	4502.9	23.7	20.5	68.7	741.2	14.9
50.9	Fr 6-I	7.39E-05	6237.7	18.7	16.7	214.4	2196.7	17.9
	# Samples	**26**	**26**	**26**	**26**	**26**	**26**	**26**
	Average	9.8E-04	5966.2	30.2	14.9	140.7	973.0	14.8
	Standard deviation	1.6E-03	1361.3	8.7	8.8	58.3	661.4	3.3
	Coeff. of variation [%]	1.7E+00	22.8	28.7	59.1	41.4	68.0	22.1
	Minimum	7.3E-06	3824.1	14.7	0.0	52.9	163.6	9.7
	Maximum	6.6E-03	8642.8	47.9	29.0	277.2	2744.7	21.0
	Range	6.6E-03	4818.7	33.2	29.0	224.3	2581.1	11.3
	Standardized bias	4.73	0.92	0.54	-1.16	1.31	2.39	0.26
	RBC	N.A.	26	40	N.A.	25	64	2.7
	MPL	N.A.	400	78	1600	N.A.	N.A.	N.A.
	AEF	N.A.	93	0.7	N.A.	2.8	50.1	5.9

http://dx.doi.org/10.18268/BSGM2024v76n3a230124

3.2. PHYSICOCHEMICAL RESULTS

The El Fraile I presents an average acid pH of 3.3 through the entire vertical profile, with two markedly maximum values at 12.7 and 39.7 m-depth (Figure 8b). Figure 5a is again reproduced for comparison purposes.

While pH is the measurement of a specific ion (*i.e.*, hydrogen) within a sample, EC is a non-specific measurement of the concentration of both positively and negatively charged ions within it. As shown in Figure 8c, EC shows a mirrored trend to that of pH. This opposite behavior could be likely explained by considering that the presence of any hydrogen ions present in a substance will affect the pH level and, most probably, also influence conductivity levels. Nevertheless, hydrogen ions make up only a small part of the ion concentration measured by a conductivity meter.

3.3. GEOCHEMISTRY RESULTS

Heavy metal elemental composition variations correlate, in general, with that of κ_{LF}; peak/trough values in half of the elements correspond to κ_{LF} peak/trough values, except for V, Ni, and Zn. Those of Pb, Ni, and Zn show significant variations. On the contrary, within the lowermost κ stable trend (34.5-50.9 m-depth), all elemental compositions show a uniformly increasing or decreasing trend, except Ni, which remains almost constant (Figure 9b-g). Worth noting is the high total Fe values, between 10 and 20 wt./%, throughout the entire vertical profile.

Following Talavera-Mendoza *et al.* (2005), metal concentrations of tailings are compared against regional background concentrations (RBC) of crop soils to estimate enrichment ratios of tailings relative to regional pristine soils. Through this comparison (Table 2), it is evident that the El Fraile I tailings are highly enriched in all reported elements −mainly in Pb and Zn−, except in V. A summary of the elemental composition and the corresponding statistical description of κ_{LF} and PTEs concentration in the El Fraile I tailing samples is presented in Table 2.

4. Discussion

Both low- and high-coercivity minerals are present in the El Fraile I dam as remanence carriers, as shown by the IRM curves (Figure 4).

As evidenced from the M−T curves, magnetite, or low Ti titanomagnetite is the main responsible for the magnetization, although intermediate temperature magnetic phases are also present. Quite irreversible M−T curves are obtained in almost all samples analyzed, which suggests the formation of new magnetic mineralogy (Figure 5).

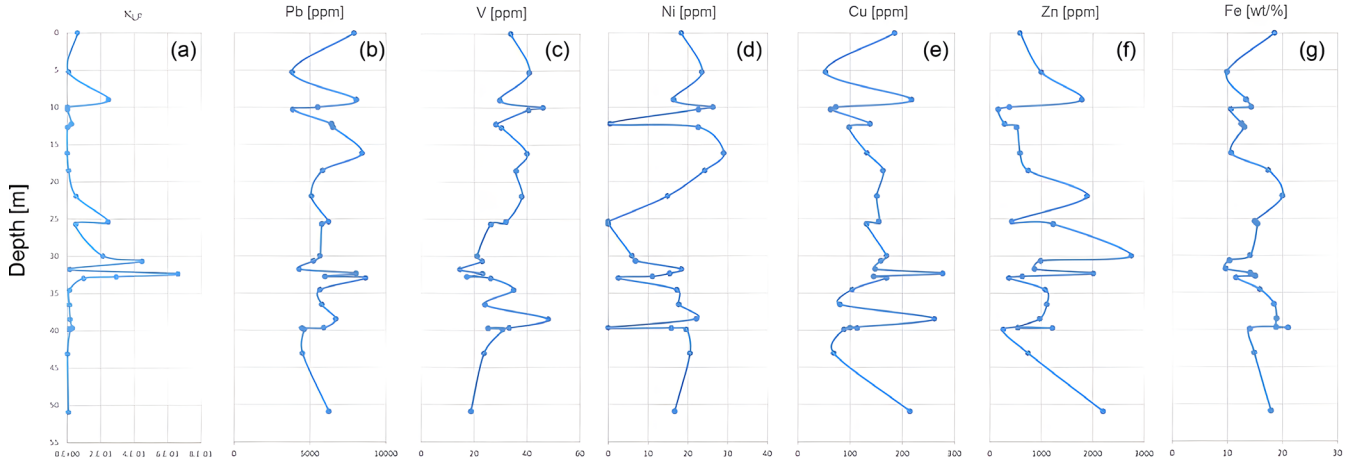

Figure 9 Associated heavy metal concentrations through the El Fraile I profile. Figure 5a is again reproduced for comparison purposes.

http://dx.doi.org/10.18268/BSGM2024v76n3a230124

Table 3. Correlation matrix. Concentration values in mg/kg, except for Fe [wt./%]. Cell's colors reflect the correlation factor value between the corresponding parameters; Green means a total correlation (1.000), while red a total inverse correlation (-1.000). Intermediate colors meaning lower than ± 1.000.

	Depth [m]	κ_{LF}	κ_{FD}%	ARM [A/m]	SRIM [A/m]	S_{-300} [A/m]	SRIM/κ_{LF} [A/m]	ARM/κ_{LF} [A/m]	SRIM/ARM [unitless]	pH	EC [µs/cm]	Pb	V	Ni	Cu	Zn	Fe
Depth [m]	1.0000																
XLF	0.0769	1.0000															
κ_{LF}	-0.3376	-0.3830	1.0000														
ARM	0.3059	0.6712	-0.2544	1.0000													
SRIM	0.2319	0.9425	-0.4522	0.7094	1.0000												
S_{-300}	0.1999	0.3672	-0.7986	0.0512	0.4597	1.0000											
SRIM/κ_{LF}	0.2423	-0.4589	0.0384	-0.2207	-0.2103	0.0791	1.0000										
ARM/κ_{LF}	-0.1397	-0.2875	0.6205	-0.1424	-0.2952	-0.6024	0.4306	1.0000									
SRIM/ARM	0.1682	0.5239	-0.6544	0.0486	0.5690	0.7254	-0.0383	-0.4342	1.0000								
pH	-0.1211	-0.2908	0.2360	0.0024	-0.1909	0.0363	0.4872	0.1883	-0.2190	1.0000							
EC	0.1594	0.2294	-0.0384	-0.0350	0.0973	-0.1156	-0.6507	-0.2550	0.1072	-0.7435	1.0000						
Pb	-0.1547	0.3238	-0.0251	0.3596	0.2581	0.0994	-0.1250	0.2158	0.0482	-0.0409	-0.2175	1.0000					
V	-0.4855	-0.3743	0.0776	-0.4722	-0.3223	0.0203	0.3594	0.2262	-0.0877	0.1243	-0.3483	0.0183	1.0000				
Ni	-0.2398	-0.3250	0.3186	-0.2905	-0.3079	-0.3692	0.4365	0.4782	-0.3393	0.1333	-0.1774	-0.1320	0.4250	1.0000			
Cu	0.1535	0.5548	-0.3172	0.5213	0.5159	0.2908	-0.3201	-0.1844	0.2743	-0.2438	0.1601	0.6288	-0.1746	-0.1669	1.0000		
Zn	0.2641	0.3637	-0.2779	0.1315	0.3529	0.2587	-0.2973	-0.2328	0.3279	-0.3278	0.5951	0.0784	-0.3396	-0.0839	0.4985	1.0000	
Fe	0.3515	-0.1845	-0.4635	-0.0813	-0.0247	0.5874	0.3238	-0.2806	0.2066	0.1311	-0.0464	0.0250	0.0858	-0.0587	0.1909	0.2612	1.0000

A general fining of the magnetic grain size at the first third part (top up to 20 m depth) is evidenced by the ARM/κ_{LF} plot (Figure 6c).

Magnetic susceptibility (and SIRM, as well) vertical survey stands out different layers of variable ferrimagnetic mineral concentration or composition, in good agreement with the stratigraphic column. However, the concentration-independence character of the SIRM/κ_{LF} points to grain size or mineralogical differences rather than concentration variations as the cause of the observed trends (Figure 6d).

As in the case of the ARM/κ_{LF} plot, a general fining of the magnetic grain size is evidenced by the κ_{FD}% plot and the S_{-300} ratio values for the same section (first upper part of the sequence) (Figure 6e).

The results above mentioned highlight the usefulness of the magnetic methods as a proxy for stratigraphy and mineral concentration of a depositional sequence.

The old dam's long evolution period could be suggested by the variable and significantly low value of the S_{-300} ratio (high oxidation degree of the magnetic mineralogy) and the mostly acid pH character throughout the whole dam.

As noted above, peak values in half of the elements correspond to κ_{LF} peak values throughout the whole deposit, although at the lowermost κ stable trend (34.5-50.9 m-depth), all elemental compositions show a uniformly increasing or decreasing trend.

Because of the scarce number of rock-magnetic investigations on this kind of anthropogenic origin systems, no regional background concentration (RBC) for κ is available for this investigation, precluding the estimation of an average enrichment factor (AEF). Nonetheless, considering the complex metal speciation within the layers (sulfides and/or sulfosalts), an estimation of an AEF would be likely nonsense.

As seen in Table 2, Pb, Cu, and Zn are the elements with a major variability within the profile (range of 4818.7, 224.3, and 2581.1, respectively). Pb and Zn are the elements with a significantly average enrichment factor (AEF).

From Table 3, the strong positive correlation between κ_{LF} and SIRM (cc = 0.9425) suggests either that a single magnetic mineral is responsible for carrying the SIRM, causing the κ_{LF} in the samples, or that the dominant minerals were in constant proportions throughout the different layers (Thompson *et al.*, 1975).

The general fining of the magnetic grain size observed in Figure 6c is corroborated by the strong positive correlation coefficient (cc = 0.6205) between κ_{FD}% and ARM/κ_{LF}.

As expected, a strong negative correlation exists

http://dx.doi.org/10.18268/BSGM2024v76n3a230124

between pH and EC.

Also observed from Table 3 is a moderate negative correlation (cc = -0.4635) between κ_{FD}% and Fe. As mentioned by Kanu *et al.* (2017), "*The significant negative correlation between Fe and κ_{FD}% further confirmed that Fe is of anthropogenic origin*." As well, from Table 3, κ_{LF}, ARM, and SIRM could be used as a proxy for V, according to the negative correlation coefficients obtained (-0.3743, -0.4722, and -0.3223, respectively). Similarly, most magnetic parameters seem to be good enough proxies for the evaluation of Ni, Cu, and Zn. A strong direct correlation between Pb and Cu contents is evident from the results presented in the matrix correlation (Table 3). Because of its long evolution period, health hazards are mainly due to the high Pb, Cu, and Zn concentrations.

As mentioned in the introduction, the El Fraile I impoundment is located 5 km SW of Taxco de Alarcón, and one could be tempted to think that the pollution problem is confined to the dam's surroundings. However, there is an adjacent problem directly linked to particulate matter (PM), the material accumulated in the dams; street dust (SD) pollution. SD is mainly composed of particles derived from anthropic processes (Dearing *et al.*, 1996). As stated in Morales *et al.* (2020), "*SD consists of a heterogeneous assortment of materials; some originated from natural processes…*", but also from "*Anthropic activities…, which is later released to the environment.*".

Fine particles of anthropic origin, particulate matter 10 μm in diameter or less (the so-called PM10 particles), are hosted by the SD, which contain magnetic minerals and traces of heavy metals (Cr, Cu, Pb, Zn, etc.) (Bautista *et al.*, 2018). Due to their particular size and shape, PM10 particles can be inhaled by humans, which is why SD is considered a significant source of breathable air pollution (Amato *et al.*, 2014).

5. Conclusions

The results presented agree with those of previous studies. However, the systematic sampling distribution employed in this investigation enables us to obtain a broader view of the concentration and distribution within these deposits.

Considering that tailings of abandoned mining districts in Mexico are nowadays occupied and serve as settlements for various inhabitant groups (Hernández-Bernal *et al.*, 2016), the study of the distribution and concentration of PTEs contained in mining wastes is currently an issue of significant relevance, as properly noted by Talavera-Mendoza *et al.* (2006). Unfortunately, as properly mentioned by Morales *et al.* (2023), "*…waste impoundments are, at least in Mexico, unattended entities…*" and "*…neither a government nor a particular company would invest time, effort, and economic resources to investigate the dam's internal structure*". This fact highlights the usefulness of magnetic susceptibility, and associated magnetic parameters, as a proxy for the investigation of waste dams.

Simple (and non-destructive) sample preparation, and fast rock-magnetic and elemental concentration estimations, together with a suitable systematic sampling distribution, make XRF measurements an advantageous proxy method for a quick and cost-effective evaluation of contamination by heavy metals.

List of abbreviations

IRM: isothermal remanent magnetization

$IRM_{-0.3\,T}$: backfield magnetization at 300 mT

PTEs: potentially toxic elements

SIRM: saturation isothermal remanent magnetization

TMD: Taxco Mining District

Wt./%: weight percent

κ_{FD}%: percent frequency-dependent magnetic susceptibility

κ_{HF}: magnetic susceptibility measurements at high frequency

κ_{LF}: magnetic susceptibility measurements at low frequency

EC: electrical conductivity

http://dx.doi.org/10.18268/BSGM2024v76n3a230124

Availability of data and materials

The datasets used and/or analyzed during the current study are available from the corresponding author upon reasonable request.

Contributions of authors

MS and JM contributed to conceptualization. NP and JM contributed to the methodology. JM carried out the fieldwork. JM and NP performed formal analysis. JM contributed to writing—original draft preparation. All authors contributed to writing—review, and editing. MS acknowledges the support of UNAM-PAPIIT Project IA102413.

Financing

No funding was received.

Acknowledgements

We thank María Felicidad Bogaló and an anonymous reviewer for their constructive comments and suggestions, which definitively improved the scientific content and the manuscript presentation. Undergraduate student Julio Gómez Rivera is acknowledged for his participation in the fieldwork and laboratory measurements.

Conflicts of interest

The author(s) declare(s) that they have no competing interests.

Handling editor

Claudia Gogorza.

References

Aguilera, A., Morales, J.J., Goguitchaichvili, A., García-Oliva, F., Armendariz-Arnez, C., Quintana, P., Bautista, F., 2020, Spatial distribution of magnetic material in urban road dust classified by land use and type of road in San Luis Potosí, Mexico: Air Quality, Atmosphere & Health, 13, 951-963. https://doi.org/10.1007/s11869-020-00851-5

Amato, F., Cassee, F.R., van der Gon, H.A.C.D., Gehrig, R., Gustafsson, M., Hafner, W., Harrison, R.M., Jozwicka, M., Kelly, F.J., Moreno, T., Prevot, A.S., Schaap, M., Sunyer, J., Querol, X., 2014, Urban air quality: the challenge of traffic non-exhaust emissions: Journal of Hazardous Materials, 275, 31-36. https://doi.org/10.1016/j.jhazmat.2014.04.053

Armienta M.A., Talavera O., Morton O., Barrera M., 2003, Geochemistry of Metals from Mine Tailings in Taxco, Mexico: Bulletin of Environmental Contamination and Toxicology, 71, 387-393. https://doi.org/10.1007/s00128-003-0176-0

Bautista, F., Gonsebatt, M.E., Cejudo, R., Goguitchaichvili, A., Delgado, M.C., Morales, J.J., 2018, Evidence of small ferrimagnetic concentrations in mice (Mus musculus) livers and kidneys exposed to the urban dust: a reconnaissance study: Geofísica Internacional, 57(1), 79-86. https://doi.org/10.22201/igeof.00167169p.2018.57.1.1824

Corona-Chávez, P., Uribe Salas, J.A., Razo Pérez, N., Martínez Medina, M., Maldonado Villanueva, R., Ramos Arroyo, Y.R., Robles Camacho, J., 2010, The impact of mining in the regional ecosystem: the Mining District of El Oro and Tlalpujahua, Mexico: De Re Metallica, 15, 21-34.

Dearing, J.A., Dann, R.J.L., Hay, K., Lees, J.A., Loveland, P.J., Maher, B.A., O'Grady, K., 1996, Frequency-dependent susceptibility measurements of environmental materials: Geophysical Journal International, 124(1), 228-240. https://doi.org/10.1111/j.1365-246X.1996.tb06366.x

Dótor-Almazán, A., Armienta-Hernández, M.A., Talavera-Mendoza, O., Ruiz, J.,

2017, Geochemical behavior of Cu and sulfur isotopes in the tropical mining region of Taxco, Guerrero (southern Mexico): Chemical Geology, 471, 1-12. https://doi.org/10.1016/j.chemgeo.2017.09.005

Ďurža, O., 1999, Heavy metals contamination and magnetic susceptibility in soils around metallurgical plant: Physics and Chemistry of the Earth, Part A: Solid Earth and Geodesy, 24(6), 541-543. https://doi.org/10.1016/S1464-1895(99)00069-1

Evans M.E, Heller F., 2003, Environmental magnetism - Principles and Applications of Enviromagnetics: San Diego, California, Academic Press, 299 p.

Hernández-Bernal, M.S., Morales, J., Corona-Chávez, P., Gogichaishvili, A., Bautista, F., 2016, Combined rock-magnetic and geochemical characterization of Angangueo mining district, central Mexico: Environmental Earth Sciences, 75, 1287. https://doi.org/10.1007/s12665-016-6097-0

Kanu, M.O., Basavaiah, N., Meludu, O.C., Oniku, A.S., 2017, Investigating the potential of using environmental magnetism techniques as pollution proxy in urban road deposited sediment: International Journal of Environmental Science and Technology, 14, 2745-2758. https://doi.org/10.1007/s13762-017-1356-5

Maldonado, B., Rehren, T., 2009, Early copper smelting at Itziparátzico, Mexico: Journal of Archaeological Science, 36(9), 1998-2006. https://doi.org/10.1016/j.jas.2009.05.019

Matasova, G.G., Kazansky, A.Y., Bortnikova, S.B., Airijants, A.A., 2005, The use of magnetic methods in an environmental study of áreas polluted with non-magnetic wastes of the mining industry (Salair region, Western Siberia, Russia): Geochemistry: Exploration, Environment, Analysis, 5, 75-89. https://doi.org/10.1144/1467-7873/03-058

Méndez, M., Armienta, M., 2012, Distribución de Fe, Zn, Pb, Cu, Cd y As originada por residuos mineros y aguas residuales en un transecto del Río Taxco en Guerrero, México: Revista Mexicana de Ciencias Geológicas, 29(2), 450-462.

Morales, J., Hernández-Bernal, M.S., Corona-Chávez, P., Gogichaishvili, A., Bautista, F., 2016, Further evidence for magnetic susceptibility as a proxy for the evaluation of heavy metals in mining wastes: case study of Tlalpujahua and El Oro Mining Districts: Environmental Earth Sciences, 75, 309, https://doi.org/10.1007/s12665-015-5187-8

Morales, J., Aguilera, A., Bautista, F. Cejudo, R., Goguitchaichvili, A., Hernández-Bernal, M.S., 2020, Heavy metal content estimation in the Mexico City Street dust: an inter-method comparison and Pb levels assessment during the last decade: SN Applied Sciences, 2, 1841. https://doi.org/10.1007/s42452-020-03647-5

Morales, J., Hernández Bernal, M.S., Pérez Rodríguez, N., Goguitchaichvili, A., 2023, Magnetic Susceptibility Prospecting and Geochemical Characterization of Taxco's Mining Waste Dam Guerrero I (Mexico): Quaternary, 6(3), 40. https://doi.org/10.3390/quat6030040

Pérez, I., Romero, F.M., Zamora, O., Gutiérrez-Ruiz, M.E., 2014, Magnetic susceptibility and electrical conductivity as a proxy for evaluating soil contaminated with arsenic, cadmium and lead in a metallurgical area in the San Luis Potosi State, Mexico: Environmental Earth Sciences, 72, 1521-1531. https://doi.org/10.1007/s12665-014-3057-4

Petrovsky, E., Kapicka, A., Zapletal, K., Sebestova, E., Spanila, T., Dekkers, M.J., Rochette, P., 1998, Correlation between magnetic parameters and chemical composition of lake sediments from Northern Bohemia—preliminary study: Physics and Chemistry of the Earth, 23(9-10), 1123-1126. https://doi.org/10.1016/S0079-1946(98)00139-6

Petrovsky, E., Kapicka, A., Jordanova, N., Boruvka,

L., 2001, Magnetic properties of alluvial soils contaminated with lead, zinc and cadmium: Journal of Applied Geophysics, 48(2), 127-136. https://doi.org/10.1016/S0926-9851(01)00085-4

Pollard, H.P., 1987, The Political Economy of Prehispanic Tarascan Metallurgy: American Antiquity, 52(4), 741-752. https://doi.org/10.2307/281382

Ramos-Arroyo, Y.R., Prol-Ledesma, R.M., Siebe-Grabach, C., 2004, Características geológicas y mineralógicas e historia de extracción del Distrito de Guanajuato, México. Posibles escenarios geoquímicos para los residuos mineros: Revista Mexicana de Ciencias Geológicas, 21(2), 268-284.

Shu, J., Dearing, J.A., Morse, A.P., Yu, L.Z., Yuan, N., 2001, Determining the sources of atmospheric particles in Shanghai, China, from magnetic and geochemical properties: Atmospheric Environment, 35(15), 2615-2625. https://doi.org/10.1016/S1352-2310(00)00454-4

Secretaría de Economía, 2024, Minería (en línea): México, Gobierno de México, disponible en <https://www.gob.mx/se/acciones-y-programas/mineria>, consultado 22 de febrero de 2024.

Secretaría de Medio Ambiente y Recursos Naturales (SEMARNAT), 2007, Norma Oficial Mexicana que establece los criterios para determinar las concentraciones de remediación de suelos contaminados por arsénico, bario, berilio, cadmio, cromo hexavalente, mercurio, níquel, plata, plomo, selenio, talio y/o vanadio (NOM-147-SEMARNAT/SSA1-2004): México, D.F., Diario Oficial de la Federación, 2 de marzo de 2007, 62 p., disponible en <https://www.gob.mx/profepa/documentos/norma-oficial-mexicana-nom-147-semarnat-ssa1-2004>

Talavera Mendoza, O., Yta, M., Moreno Tovar, R., Dótor Almazán, A., Flores Mundo, N., Duarte Gutiérrez, C., 2005, Mineralogy and geochemistry of sulfide-bearing tailings from silver mines in the Taxco, Mexico area to evaluate their potential environmental impact: Geofísica Internacional, 44(1), 49-64. https://doi.org/10.22201/igeof.00167169p.2005.44.1.552

Talavera-Mendoza, O., Armienta, M., García, J., Flores, N., 2006, Geochemistry of leachates from the El Fraile I sulfide tailings piles in Taxco, Guerrero, southern Mexico: Environmental Geochemistry and Health, 28, 243-255. https://doi.org/10.1007/s10653-005-9037-6

Talavera-Mendoza, O., Ruiz, J., Díaz-Villaseñor, E., Ramírez-Guzmán, A., Cortés, A., Salgado-Souto, S.A., Dótor-Almazán, A., Rivera-Bustos, R., 2016, Water-rock-tailings interactions and sources of sulfur and metals in the subtropical mining region of Taxco, Guerrero (southern Mexico): a multi-isotopic approach: Applied Geochemistry, 66, 73-81. https://doi.org/10.1016/j.apgeochem.2015.12.002

Thompson, R., Battarbee, R., O'Sullivan, P.E., Oldfield, F., 1975, Magnetic susceptibility of lake sediments. Limnology and Oceanography, 20(5), 687-698.

Thompson, R., Stober, J.C., Turner, G.M., Oldfield, F., Bloemendal, J., Dearing, J.A., Rummery, T.A., 1980, Environmental Applications of Magnetic Measurements: Science 207(4430), 481-486. https://doi.org/10.1126/science.207.4430.481

Thompson, R., Oldfield, F., 1986, Environmental Magnetism: London: Allen & Unwin, 237 p. http://dx.doi.org/10.1007/978-94-011-8036-8

Vigliotti, L., Verosub, K.L., Cattaneo, A., Trincardi, F., Asioli, A., Piva, A., 2008, Palaeomagnetic and rock magnetic analysis of Holocene deposits from the Adriatic Sea: detecting and dating short-term fluctuations in sediment supply: The Holocene, 18(1), 141-152. http://dx.doi.org/10.1177/0959683607085605